Results in Physics 68 (2025) 108081

Contents lists available at ScienceDirect

Results in Physics

journal homepage: www.elsevier.com/locate/rinp

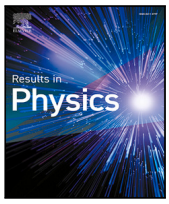

Microwave spectroscopy assisted by electromagnetically induced transparency near natural Förster resonance on Rubidium

Naomy Duarte Gomes [a], Daniel Varela Magalhães [a], J.D. Massayuki Kondo [a,b], Luis Gustavo Marcassa [a,*]

[a] Instituto de Física de São Carlos, Universidade de São Paulo, Av. Trab. São Carlense, 400 - Parque Arnold Schimidt, São Carlos, 13566-590, SP, Brazil
[b] Departamento de Física, Universidade Federal de Santa Catarina, R. Eng. Agronômico Andrei Cristian Ferreira, s/n - Trindade, Florianópolis, 88040-900, SC, Brazil

ARTICLE INFO

Keywords:
Microwave sensor
EIT
Förster resonance
Quantum defect
Microwave spectroscopy

ABSTRACT

In this work, we precisely measure the transition energies between the Rydberg state $nD_{5/2}$ to the nearby Rydberg states $(n+2)P_{3/2}$, $(n-2)F_{7/2}$ in ^{85}Rb for the range $41 \leq n \leq 46$. This was done by carrying out microwave spectroscopy via electromagnetically induced transparency (EIT) in a room temperature vapor reference cell of rubidium, which is similar to the experimental approach followed by Li et al., (2021). This range is interesting because there is a quasi Förster resonance between the atomic pair $43D_{5/2} + 43D_{5/2}$ and $45P_{3/2} + 41F_{7/2}$. We compared the obtained results with numerically calculated transition energies based on previously tabulated quantum defect numbers by various research groups using both hot and ultra-cold atomic samples. Our data are more consistent with measurements made within ultra-cold atomic systems (Li et al., 2003; Han et al., 2006).

Introduction

In recent years, the exploration of the unique properties of highly excited Rydberg atoms has become pivotal for advancing several quantum technologies, spanning from quantum information [1,2], computation [3,4], simulation [5,6], highly sensitive electromagnetic sensors [7–12], to understanding the physical background behind non-equilibrium phase transitions in hot atomic vapors [13,14]. These inquiries also extend to the characterization of many fundamental atomic properties, such as atomic lifetime [9], and quadrupolar polarizability information of the alkali ionic core [15–17]. In order to explore the highly precision state energies and transition energies embedded in Rydberg atomic states, fundamental information is imperative, specifically their intrinsic transition dipole moments (μ_d), which play a central role in electromagnetic sensing and entanglement protocols based on Rydberg–Rydberg interactions [18–20]. The calculation of these precise energies of Rydberg transitions is paramount in predicting accurately the behavior of atomic or molecular samples under study.

Rydberg energy spectra (E_n) in alkali atomic samples involves an effective quantum number (n^*) and it is given by:

$$E_n = \frac{R_y c}{n^{*2}}, \tag{1}$$

where R_y is the Rydberg constant, c is the speed of light, and $n^* = n - \delta_{n,l,j}$, where the deviation $\delta_{n,l,j}$, is known as quantum defect [21], and is experimentally obtained. Quantum defects exhibits a dependence on the orbital and total angular momentum (l, j) and a slight dependence on the principal quantum number n and it is expressed through the modified Rydberg–Ritz coefficients as [21]:

$$\delta_{n,l,j} \approx \delta_0 + \frac{\delta_2}{(n - \delta_0)^2}, \tag{2}$$

where δ_0 and δ_2 are constant coefficients experimentally tabulated for each orbital angular momentum quantum number l and the total angular momentum j when accessible.

Numerous research groups have systematically measured quantum defects for various alkali atomic samples [21]. The works of Wenhui Li et al. [22] and Jianing Han et al. [23] providing a comprehensive set for ^{85}Rb. They meticulously tabulated quantum defects for $nS_{1/2}$, $nP_{1/2,3/2}$, $nD_{3/2,5/2}$, $nF_{5/2,7/2}$, using an ultra-cold sample held within a magneto-optical trap. Other research groups have measured quantum defects for ^{85}Rb using thermal atoms. Sanguinetti et al. [24] applied field ionization technique in an atomic beam for $nP_{3/2}$ states. Johnson et al. [25] used vapor cell absorption spectroscopy for $nF_{7/2}$ states. Shaohua Li et al. [26] used microwave (MW) assisted electromagnetically induced transparency (EIT), starting from the $nD_{5/2}$ state, for $nP_{3/2}$ and $nF_{7/2}$ states. Such thermal atom works reveal slightly

* Corresponding author.
E-mail address: marcassa@ifsc.usp.br (L.G. Marcassa).

https://doi.org/10.1016/j.rinp.2024.108081
Received 27 June 2024; Received in revised form 2 December 2024; Accepted 10 December 2024
Available online 17 December 2024
2211-3797/© 2024 The Authors. Published by Elsevier B.V. This is an open access article under the CC BY license (http://creativecommons.org/licenses/by/4.0/).

different quantum defects when compared among themselves and with the cold samples results.

A pair of $43D_{5/2}$ Rydberg atoms contains a natural Förster resonance where the atomic pairwise energy $43D_{5/2}+43D_{5/2}$ has an almost degenerate energy with the $45P_{3/2}+41F_{7/2}$ atomic pair for a zero electric field, leading to strong dipole Rydberg–Rydberg two-body interactions [27]. This is analogous to Förster resonance energy transfer (FRET), which is a mechanism of energy transfer between two light-sensitive molecules without photon emission. It has been proposed that such a process may be used for the implementation of quantum gates, allowing precise control of the qubit [28].

In this work, we present a spectroscopic analysis built up via EIT using two optical photons and one microwave photon to obtain the energy spectrum of Rydberg states for ^{85}Rb. Specifically, we explore the states $(n+2)P_{3/2}$ and $(n-2)F_{7/2}$, which can be coupled with the initial target Rydberg state $nD_{5/2}$ for $41 \leq n \leq 46$. We carried directly measurements of energy differences for a natural Förster resonance at n=43, which are compared with theoretical values using quantum defects already tabulated in the literature [22–26]. Our findings show closer alignment with measurements conducted using ultra-cold atomic samples [22,23].

Experimental setup and methods

The experimental setup used in this study follows the design described in [29]. Clearly, adjustments and modifications were introduced, tailoring the setup to the unique requirements of our research questions and enhancing experimental precision, as shown in Fig. 1. In brief, we used a 75 mm Rb vapor reference cell at room temperature. A diode laser at 780 nm couples the ground state to the intermediate state $5S_{1/2},(F=3) \rightarrow 5P_{3/2},(F'=4)$; this is called the probe beam and operates in the weak regime when its intensity is much lower than the transition saturation intensity. A second laser operating at 480 nm couples the intermediate state to the first initial target Rydberg state $5P_{3/2},(F=4) \rightarrow nD_{5/2}$ [30] and is called the coupling beam. Both optical beams are frequency locked at zero detuning, using a thermally stabilized home-made Fabry–Perot optical cavity [31], with laser linewidths of 100 kHz. The microwave photon is generated by an eightfold circuit consisting of a passive doubler (Model ZX90-2-24-S+ from Minicircuits) and quadrupler (Model 934VF-10/385 from Mi-Wave), producing frequencies in the range of 50 to 75 GHz. This circuit connects the initial Rydberg target state to nearby Rydberg states $nD_{5/2} \rightarrow (n+2)P_{3/2}$ and $(n-2)F_{7/2}$ through a dipole one-photon transition. The MW signal is provided by a commercial two-channel MW generator (Windfreak Technologies, model SynthPRO). To improve the signal-to-noise ratio, the probe beam optical signal is processed by a lock-in amplifier at 1 kHz modulation of the microwave field. A round horn antenna (Model WR15 UG-385/U-Pasternack) feeds the MW to the atoms and is positioned at a distance of 40 cm from the experimental cell to obtain quasi-plane wave microwave radiation.

The optical beams counter-propagate and are all linearly polarized in the same direction, overlapping at the center of the cell with a 180 μ m waist. The probe laser Rabi frequency is $\Omega_p = 2\pi \times 2.32$ MHz and is constantly monitored by a photodiode. The coupling laser has $\Omega_d = 2\pi \times 3.56$ MHz. The MW photon Rabi frequency is $\Omega_{MW} = 2\pi \times 0.5$ MHz and is orthogonally aligned in respect to the vapor cell, probe, and coupling beams and it is unpolarized. The MW power was calibrated using the Autler-Townes splitting for each transition. Fig. 2 shows experimental EIT spectra for the $43P_{3/2}$ and $39F_{7/2}$ coupled to the initial Rydberg target state $41D_{5/2}$ as a function of the MW frequency. Since the probe and coupling laser frequencies are locked at two-photon EIT resonance, the MW disrupts the EIT signal, decreasing the transmission on resonance (through the Autler Townes effect). Due to the used lock-in technique, such effect is observed as a peak in Fig. 2.

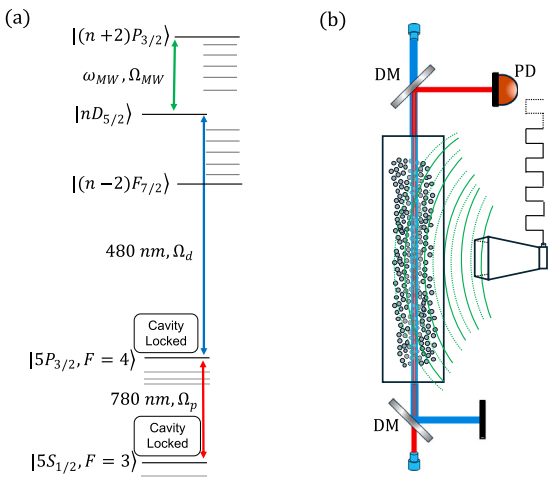

Fig. 1. (a) Energy level diagram for MW spectroscopy using EIT, (b) Rb reference cell, horn microwave antenna, dichroic mirror (DM) and photodiode (PD).

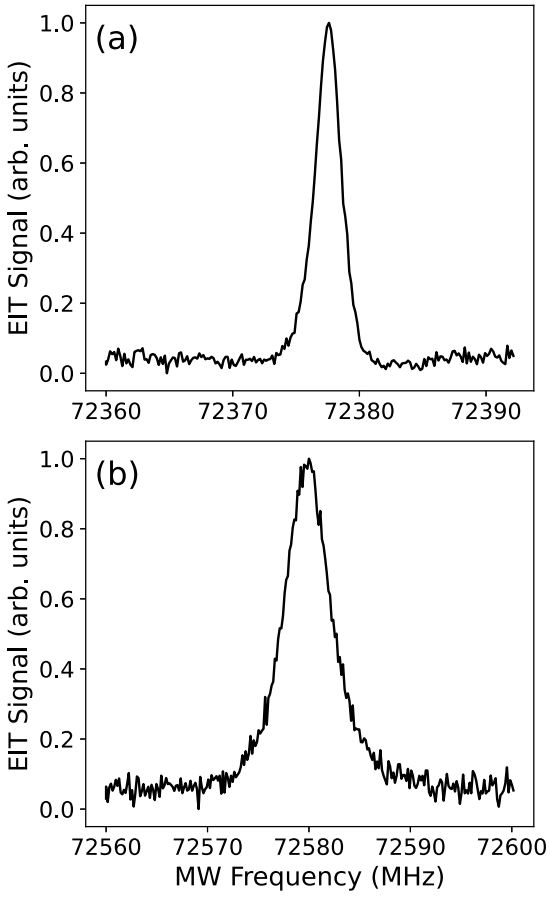

Fig. 2. EIT typical spectra as a function of the MW frequency: (a) $41D_{5/2} \rightarrow 43P_{3/2}$, (b) $41D_{5/2} \rightarrow 39F_{7/2}$.

Experimental analysis and discussion

We have measured the following transition frequencies between the initial Rydberg target state $nD_{5/2}$ and the final states for the range of principal quantum numbers $41 \leq n \leq 46$ (see Eqs. (3) and (4)). The main sources of error for the transition frequency measurements are the frequency positions of the EIT peaks and the instabilities in the lock of the probe and coupling lasers. Both lasers are frequency-stabilized

Table 1
Transition frequencies from $nD_{5/2} \rightarrow (n+2)P_{3/2}$ measured in this work are compared with the calculated transition frequencies using quantum defects tabulated by W. Li et al. [22]. The relative deviation is also shown.

n	$\nu_{nD_{5/2},(n+2)P_{3/2}}$ (MHz)	$\nu_{nD_{5/2},(n+2)P_{3/2}}$ W. Li et al. [22]	Relative deviation ($\times 10^{-5}$)
41	72377 ± 1	72378.38 ± 0.11	−1.9 ± 1.5
42	67212 ± 1	67213.37 ± 0.11	−2.0 ± 1.6
43	62527 ± 1	62528.29 ± 0.10	−2.0 ± 1.7
44	58267 ± 1	58268.68 ± 0.09	−2.9 ± 1.9
45	54386 ± 1	54387.31 ± 0.08	−2.4 ± 2.0
46	50844 ± 1	50843.13 ± 0.08	1.7 ± 2.1

Table 2
Transition frequencies from $nD_{5/2} \rightarrow (n-2)F_{7/2}$ measured in this work are compared with the calculated transition frequencies using quantum defects tabulated by J. Han et al. [23]. The relative deviation is also shown.

n	$\nu_{nD_{5/2},(n-2)F_{7/2}}$ (MHz)	$\nu_{nD_{5/2},(n-2)F_{7/2}}$ J. Han et al. [23]	Relative deviation ($\times 10^{-5}$)
41	72579 ± 1	72577.46 ± 0.52	2.1 ± 2.1
42	67310 ± 1	67308.01 ± 0.46	3.0 ± 2.2
43	62538 ± 1	62536.62 ± 0.41	2.2 ± 2.2
44	58209 ± 1	58205.80 ± 0.36	5.5 ± 2.3
45	54269 ± 1	54265.85 ± 0.32	5.8 ± 2.4
46	50675 ± 1	50673.64 ± 0.29	2.7 ± 2.5

using an optical cavity, with a frequency instability of 100 kHz. The optical cavity itself exhibits a 50 kHz drift per hour. Based on multiple measurements, the standard deviation is 1 MHz for the P and F Rydberg states in the determination of the peak positions, which were obtained by fitting the spectra with Lorentzian function. This standard deviation dominates over other errors and will be considered as the maximum error in this work.

$$nD_{5/2} \rightarrow (n+2)P_{3/2}. \quad (3)$$

$$nD_{5/2} \rightarrow (n-2)F_{7/2}. \quad (4)$$

The experimental transition frequencies can be compared to calculated ones, $\nu_{nn'}$, using Eq. (5), where n and n' represent the initial target Rydberg state, $nD_{5/2}$, and any final state, respectively.

$$\nu_{nn'} = R_y c \left(\frac{1}{(n-\delta_{n,l,j})^2} - \frac{1}{(n'-\delta_{n',l',j'})^2} \right). \quad (5)$$

Where $R_y = 109736.605\ cm^{-1}$ is the Rydberg constant for ^{85}Rb, $c = 2.99792458 \times 10^{10}$ cm/s is the speed of light. $\delta_{n,l,j}$ was calculated through Eq. (2), using δ_0 and δ_2 from [22,23]. It is important to note that this comparison can only be done with these references, as the authors of [22,23] specifically measured the $nD_{5/2}$ state.

Table 1 displays the experimental data alongside calculated values using quantum defects tabulated by W. Li et al. [22] for the transition $nD_{5/2} \rightarrow (n+2)P_{3/2}$. Table 2 presents a comparison of relative transition frequencies of $nD_{5/2} \rightarrow (n-2)F_{7/2}$ using quantum defects provided by J. Han et al. [23]. The relative deviation is at the order of 10^{-5}, which may be due to the fact that our experiment is performed with hot atoms, introducing broadening to the transition peaks due to the atomic velocity distribution within the sample.

We extract from the experimental transitions frequencies, the energy difference between $(n+2)P_{3/2}$ and $(n-2)F_{7/2}$ Rydberg states and present the absolute value $|\Delta_{(n+2)P-(n-2)F}|$ (second column in Table 3). This parameter was also calculated using the quantum defects obtained experimentally by W. Li and J. Han et al. [22,23], Sanguinetti and Johnson et al. [24,25], and Shaohua Li et al. [26], and are also presented in Table 3. Fig. 3 shows $|\Delta_{(n+2)P-(n-2)F}|$ obtained from this work in comparison to Refs. [22–26]. Particularly, our experimental data are in lines with the values calculated using quantum defects from W. Li and J. Han et al. [22,23], while discernibly mismatching the

Table 3
Energy difference ($|\Delta_{(n+2)P-(n-2)F}|$) measured in this work is shown below and compared with expected values using quantum defect coefficients from W. Li and J. Han et al. [22,23], Sanguinetti and Johnson et al. [24,25], and Shaohua Li et al. [26].

n	Exp. (MHz)	W. Li et al. [22] J. Han et al. [23] (MHz)	Sanguinetti et al. [24] Johnson et al. [25] (MHz)	S. Li [26] (MHz)
41	202 ± 2	199.08 ± 0.63	179 ± 8	160 ± 8
42	98 ± 2	94.65 ± 0.56	76 ± 8	58 ± 8
43	11 ± 2	8.33 ± 0.50	10 ± 8	26 ± 7
44	58 ± 2	62.88 ± 0.45	80 ± 8	95 ± 7
45	117 ± 2	121.47 ± 0.40	138 ± 8	151 ± 6
46	168 ± 2	169.49 ± 0.36	185 ± 8	197 ± 6

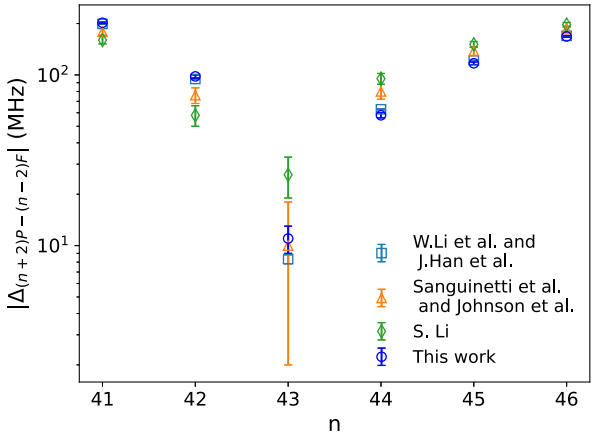

Fig. 3. The energy difference ($|\Delta_{(n+2)P-(n-2)F}|$) between $(n+2)P_{3/2}$ and $(n-2)F_{7/2}$ states as a function of n. The data acquired in this work is compared to calculated values using quantum defects coefficients obtained by W. Li and J. Han et al. [22,23], Sanguinetti and Johnson et al. [24,25] and Shaohua Li et al. [26].

values from other research groups [24–26]. A pronounced dependence on the principal quantum number n is evident in this case, due to a naturally occurring Förster resonance for n = 43 [27,32].

Fig. 4 shows the dependency of the EIT signal on the microwave radiation frequency, driving the $43D_{5/2} \rightarrow 45P_{3/2}$ and $43D_{5/2} \rightarrow 41F_{7/2}$ transitions. The measured Förster resonance energy difference is 11 ± 2 MHz, which is twice smaller than predicted by Shaohua Li et al. [26] in their available data. Furthermore, there are two differences between the experimental conditions in the two works. Firstly, Shaohua Li et al. [26] performed their measurements using a microwave Rabi frequency 20 times higher than ours, which causes power broadening and shifts the spectral lines. Their atomic transition Q factors ($Q = \nu_{nn'}/\Delta\nu_{MW}$) are about 1,000, whereas in our probed range of Rydberg states, it is 5 times larger resulting in higher accuracy. Secondly, they observed the EIT transmission signal as a function of the MW frequency by modulating the coupling laser intensity. By modulating the MW power, we were able to measure the EIT transmission signal difference with and without MW, which improved the signal-to-noise ratio.

Conclusion

In this study, we employed microwave spectroscopy assisted by EIT to measure the relative transition frequencies for Rydberg atomic energy states of ^{85}Rb. Specifically, we focus on the states $(n+2)P_{3/2}$ and $(n-2)F_{7/2}$, all originating from the initial Rydberg target state $nD_{5/2}$ near a natural occurrence of the Förster resonance. Notably, we identified the lowest energy difference due to the quasi-molecular formation of the excited Rydberg two-body system, pinpointing a natural Förster resonance at n=43, marked by an experimentally measured splitting of 11 ± 2 MHz, in excellent agreement with expected values. To validate our experimental results, we compared the relative transition

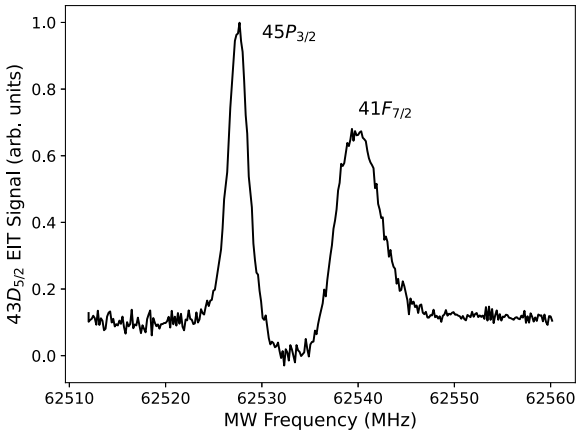

Fig. 4. Transmission signal (EIT) as a function of MW frequency, coupling $43D_{5/2} \rightarrow 45P_{3/2}$ and $43D_{5/2} \rightarrow 41F_{7/2}$ Rydberg state. The measured energy difference from Förster resonance is 11 ± 2 MHz.

frequencies with those expected, calculated using a modified Rydberg–Ritz equation, incorporating tabulated quantum defects $\delta_{l,j}$ obtained by various research groups utilizing different methods. Our conclusion is that our results strongly support the quantum defect values generated by Wenhui Li et al. [22] and Jianing Han et al. [23] using cold atomic samples. Recent quantum defect measurement in Cs suggests that better results can only be obtained using cold atomic samples and laser sources calibrated against a frequency comb locked to an atomic clock [33].

CRediT authorship contribution statement

Naomy Duarte Gomes: Writing – review & editing, Validation, Methodology, Formal analysis, Conceptualization. **Daniel Varela Magalhães:** Writing – review & editing, Resources, Investigation. **J.D. Massayuki Kondo:** Writing – review & editing, Writing – original draft, Validation, Software, Methodology, Formal analysis, Conceptualization. **Luis Gustavo Marcassa:** Writing – review & editing, Writing – original draft, Supervision, Funding acquisition, Data curation, Conceptualization.

Declaration of competing interest

The authors declare that they have no known competing financial interests or personal relationships that could have appeared to influence the work reported in this paper.

Acknowledgments

This work was supported by grants 2019/10971-0, 2021/06371-7 and 2013/07276-1 from the São Paulo Research Foundation (FAPESP), and by CNPq under grant 305257/2022-6. It was also supported by the Army Research Office under grant number W911NF-21-1-0211.

Data availability

Data will be made available on request.

References

[1] Saffman M, Walker TG, Mølmer K. Quantum information with Rydberg atoms. Rev Modern Phys 2010;82:2313–63. http://dx.doi.org/10.1103/RevModPhys.82.2313.
[2] Liu Y-M, Tian X-D, Wang J, Fan C-H, Gao F, Bao Q-Q. All-optical transistor based on Rydberg atom-assisted optomechanical system. Opt Express 2018;26(9):12330–43. http://dx.doi.org/10.1364/OE.26.012330.
[3] Cohen SR, Thompson JD. Quantum computing with circular Rydberg atoms. PRX Quantum 2021;2:030322. http://dx.doi.org/10.1103/PRXQuantum.2.030322.
[4] Saffman M. Quantum computing with neutral atoms. Nat Sci Rev 2018;6(1):24–5. http://dx.doi.org/10.1093/nsr/nwy088.
[5] Browaeys A, Lahaye T. Many-body physics with individually controlled Rydberg atoms. Nat Phys 2020;16:132–42. http://dx.doi.org/10.1038/s41567-019-0733-z.
[6] Weimer H, Müller M, Lesanovsky I, Zoller P, Büchler HP. A Rydberg quantum simulator. Nat Phys 2010;6:382–8. http://dx.doi.org/10.1038/nphys1614.
[7] Sedlacek JA, Schwettmann A, Kübler H, Löw R, Pfau T, Shaffer JP. Microwave electrometry with Rydberg atoms in a vapour cell using bright atomic resonances. Nat Phys 2012;8(11):819–24.
[8] Holloway CL, Simons MT, Gordon JA, Dienstfrey A, Anderson DA, Raithel G. Electric field metrology for SI traceability: Systematic measurement uncertainties in electromagnetically induced transparency in atomic vapor. J Appl Phys 2017;121(23):233106.
[9] Holloway CL, Gordon JA, Jefferts S, Schwarzkopf A, Anderson DA, Miller SA, Thaicharoen N, Raithel G. Broadband Rydberg atom-based electric-field probe for SI-traceable, self-calibrated measurements. IEEE Trans Antennas and Propagation 2014;62(12):6169–82.
[10] Holloway CL, Gordon JA, Schwarzkopf A, Anderson DA, Miller SA, Thaicharoen N, Raithel G. Sub-wavelength imaging and field mapping via electromagnetically induced transparency and Autler-Townes splitting in Rydberg atoms. Appl Phys Lett 2014;104(24):244102.
[11] Fan H, Kumar S, Sedlacek J, Kübler H, Karimkashi S, Shaffer JP. Atom based RF electric field sensing. J Phys B: At Mol Opt Phys 2015;48(20):202001.
[12] Sedlacek JA, Schwettmann A, Kübler H, Shaffer JP. Atom-based vector microwave electrometry using rubidium Rydberg atoms in a vapor cell. Phys Rev Lett 2013;111:063001. http://dx.doi.org/10.1103/PhysRevLett.111.063001.
[13] Carr C, Ritter R, Wade CG, Adams CS, Weatherill KJ. Nonequilibrium phase transition in a dilute Rydberg ensemble. Phys Rev Lett 2013;111:113901. http://dx.doi.org/10.1103/PhysRevLett.111.113901.
[14] Wadenpfuhl K, Adams CS. Emergence of synchronization in a driven-dissipative hot Rydberg vapor. Phys Rev Lett 2023;131:143002. http://dx.doi.org/10.1103/PhysRevLett.131.143002.
[15] Gregoire MD, Brooks N, Trubko R, Cronin AD. Analysis of polarizability measurements made with atom interferometry. Atoms 2016;4(3). http://dx.doi.org/10.3390/atoms4030021.
[16] Moore K, Duspayev A, Cardman R, Raithel G. Measurement of the Rb g-series quantum defect using two-photon microwave spectroscopy. Phys Rev A 2020;102:062817. http://dx.doi.org/10.1103/PhysRevA.102.062817.
[17] Berl SJ, Sackett CA, Gallagher TF, Nunkaew J. Core polarizability of rubidium using spectroscopy of the ng to nh, ni Rydberg transitions. Phys Rev A 2020;102:062818. http://dx.doi.org/10.1103/PhysRevA.102.062818.
[18] Wilk T, Gaëtan A, Evellin C, Wolters J, Miroshnychenko Y, Grangier P, Browaeys A. Entanglement of two individual neutral atoms using Rydberg blockade. Phys Rev Lett 2010;104:010502. http://dx.doi.org/10.1103/PhysRevLett.104.010502.
[19] Saffman M, Mølmer K. Efficient multiparticle entanglement via asymmetric Rydberg blockade. Phys Rev Lett 2009;102:240502. http://dx.doi.org/10.1103/PhysRevLett.102.240502.
[20] Urban E, Johnson TA, Henage T, Isenhower L, Yavuz DD, Walker TG, Saffman M. Observation of Rydberg blockade between two atoms. Nat Phys 2009;5:110–4. http://dx.doi.org/10.1038/nphys1178.
[21] Gallagher T. Rydberg atoms. Cambridge University Press; 2006.
[22] Li W, Mourachko I, Noel MW, Gallagher TF. Millimeter-wave spectroscopy of cold Rb Rydberg atoms in a magneto-optical trap: Quantum defects of the ns, np, and nd series. Phys Rev A 2003;67:052502. http://dx.doi.org/10.1103/PhysRevA.67.052502.
[23] Han J, Jamil Y, Norum DVL, Tanner PJ, Gallagher TF. Rb nf quantum defects from millimeter-wave spectroscopy of cold ^{85}Rb Rydberg atoms. Phys Rev A 2006;74:054502. http://dx.doi.org/10.1103/PhysRevA.74.054502.
[24] Sanguinetti B, Majeed HO, Jones ML, Varcoe BTH. Precision measurements of quantum defects in the $nP_3/2$ Rydberg states of ^{85}Rb. J Phys B: At Mol Opt Phys 2009;42(16):165004. http://dx.doi.org/10.1088/0953-4075/42/16/165004.
[25] Johnson LAM, Majeed HO, Sanguinetti B, Becker T, Varcoe BTH. Absolute frequency measurements of ^{85}Rb $nF_7/2$ Rydberg states using purely optical detection. New J Phys 2010;12(6):063028. http://dx.doi.org/10.1088/1367-2630/12/6/063028.
[26] Li S, Yuan J, Wang L, Xiao L, Jia S. Measurement of the quantum defects of ^{85}Rb P and F-series via microwave-assisted electromagnetically induced transparency spectroscopy. Results Phys 2021;29:104728. http://dx.doi.org/10.1016/j.rinp.2021.104728.

[27] Kondo JM, Gonçalves LF, Cabral JS, Tallant J, Marcassa LG. Two-body Förster resonance involving Rb nD states in a quasi-electrostatic trap. Phys Rev A 2014;90:023413. http://dx.doi.org/10.1103/PhysRevA.90.023413.

[28] Beterov II, Saffman M. Rydberg blockade, Förster resonances, and quantum state measurements with different atomic species. Phys Rev A 2015;92:042710. http://dx.doi.org/10.1103/PhysRevA.92.042710.

[29] Duarte Gomes N, da Fonseca Magnani B, Massayuki Kondo JD, Marcassa LG. Polarization spectroscopy applied to electromagnetically induced transparency in hot Rydberg atoms using a Laguerre-Gaussian beam. Atoms 2022;10(2):58.

[30] Kondo JM, Booth D, Gonçalves LF, Shaffer JP, Marcassa LG. Role of multilevel Rydberg interactions in electric-field-tuned Förster resonances. Phys Rev A 2016;93:012703. http://dx.doi.org/10.1103/PhysRevA.93.012703.

[31] Fernández DR, Torres MAL, Cardoso MR, Kondo JDM, Saffman M, Marcassa LG. Affordable medium-finesse optical cavity for diode laser stabilization. Appl Phys B 2024;130(60):60. http://dx.doi.org/10.1007/s00340-024-08190-4.

[32] Younge KC, Reinhard A, Pohl T, Berman PR, Raithel G. Mesoscopic Rydberg ensembles: Beyond the pairwise-interaction approximation. Phys Rev A 2009;79:043420. http://dx.doi.org/10.1103/PhysRevA.79.043420.

[33] Shaffer JP. Precision measurement of the energy levels and quantum defects of Cs. 2024, Private communication (unpublished).